Taylor & Francis
Taylor & Francis Group

BASIC RESEARCH PAPER

Progress of endocytic CHRN to autophagic degradation is regulated by RAB5-GTPase and T145 phosphorylation of SH3GLB1 at mouse neuromuscular junctions in vivo

Franziska Wild[a,b,c], Muzamil Majid Khan [a,b,c], Tatjana Straka[a,b], and Rüdiger Rudolf [a,b,c]

[a]Interdisciplinary Center for Neurosciences, University of Heidelberg, Heidelberg, Germany; [b]Institute of Molecular and Cell Biology, Mannheim University of Applied Sciences, Mannheim, Germany; [c]Institute of Toxicology and Genetics, Karlsruhe Institute of Technology, Eggenstein-Leopoldshafen, Germany

ABSTRACT

Endocytosed nicotinic acetylcholine receptors (CHRN) are degraded via macroautophagy/autophagy during atrophic conditions and are accompanied by the autophagic regulator protein SH3GLB1. The present study addressed the functional role of SH3GLB1 on CHRN trafficking and its implementation. We found an augmented ratio of total SH3GLB1 to threonine-145 phosphorylated SH3GLB1 (SH3GLB1:p-SH3GLB1) under conditions of increased CHRN vesicle numbers. Overexpression of T145 phosphomimetic (T145E) and phosphodeficient (T145A) mutants of SH3GLB1, was found to either slow down or augment the processing of endocytic CHRN vesicles, respectively. Co-expression of the early endosomal orchestrator RAB5 largely rescued the slow processing of endocytic CHRN vesicles induced by T145E. SH3GLB1 phosphomutants did not modulate the expression or colocalization of RAB5 with CHRN vesicles, but instead altered the expression of RAB5 activity regulators. In summary, these findings suggest that SH3GLB1 controls CHRN endocytic trafficking in a phosphorylation- and RAB5-dependent manner at steps upstream of autophagosome formation.

Introduction

Autophagy is a major proteolytic pathway known for its importance in clearing cytosolic protein aggregates, damaged mitochondria, and bacteria. However, endosomes can also fuse with autophagosomes, which leads to the formation of amphisomes.[1,2] Fusion of these amphisomes with lysosomes results in the generation of autolysosomes[1] and the hydrolysis of their cargo. The biogenesis of autophagosomes largely relies on a group of autophagy-related proteins[3] that initially relocate to source membranes, such as the phagophore assembly site in yeast[4] and different regions in mammalian cells,[5] and drive autophagosome formation in a stimulus-dependent manner. In HeLa cells SH3GLB1 (SH3 domain containing GRB2 like endophilin B1)[6] is crucial for the shuttling of the autophagosome-inducing ATG9A (autophagy-related 9A) as well as the tubulation of vesicular structures containing MAP1LC3A (microtubule-associated protein 1 light chain 3 α) and RAB5 (RAB5, member RAS oncogene family) upon autophagy induction.[7] RAB5 is a small GTPase that cycles between a membrane bound active state and a cytosolic inactive state.[8] Under normal conditions, RAB5 primarily orchestrates the endolysosomal pathway by attracting different protein complexes to early endosomes, including the vacuolar-type H$^+$-ATPase (v-ATPase).[9] Inclusion of this v-ATPase in endosomes serves the purpose of acidifying the endosomal lumen and driving its

transition from early to late endosome.[10] Recruitment of RAB5 and v-ATPase to endosomes depends on SH3GLB1 and its complex with HTATIP2 (HIV-1 Tat interactive protein 2) and ACSL4 (acyl-CoA synthetase long-chain family member 4).[9,11] Thus, SH3GLB1 is involved in both endocytic[9,11] as well as autophagic processes.[6,12-16]

SH3GLB1 is subjected to posttranslational phosphorylation at various amino acid residues,[12,17] with CDK5 (cyclin dependent kinase 5)-dependent phosphorylation of the threonine residue at position 145 having shown particular relevance for its activity in starvation-induced autophagy.[12] We have recently reported that SH3GLB1, together with the E3 ligase TRIM63 (tripartite motif containing 63), is involved in the autophagic degradation of CHRN, a heteropentameric ligand-gated ion channel, in live mouse skeletal muscle.[16,18] This process was active at basal levels, but it was markedly enhanced upon the alteration of autophagic activity by sciatic denervation, which is a model for muscle atrophy.[16] Although SH3GLB1-positive and CHRN-containing endolysosomes colocalized with different markers (TRIM63 and MAP1LC3A), it remained unclear how and at which point SH3GLB1 might regulate CHRN endocytic trafficking. In the present work, which addresses these questions, we found that a principal part of the activity of SH3GLB1 on CHRN-containing vesicles occurs at the level of early endosomes and is subject to regulation by the

phosphorylation status of SH3GLB1 at position T145. Furthermore, we observed an increased ratio of SH3GLB1:p-SH3GLB1 upon denervation, which was shown to be important for efficient processing of endocytosed CHRN.

Results

Internalized CHRN accumulate upon denervation and in the presence of chloroquine

We first studied the effects of denervation and blockage of endocytic or autophagic flux on the accumulation of internalized CHRN. Therefore, by cutting the sciatic nerve, hindlimb muscles were unilaterally denervated. After 4 d, the surface-exposed CHRN located on *tibialis anterior* (TA) muscles on both legs were stained using fluorescently labeled α-bungarotoxin-Alexa Fluor 647 (BGT-AF647), a highly specific peptide marker for CHRN, while innervated legs served as the control group. Labeled CHRN were allowed to endocytose and in vivo confocal microscopy was then performed 24 h later on these TA muscles to image the neuromuscular junction (NMJ) morphology as well as the CHRN endolysosomal carriers. In addition to control animals, one group of mice were systemically administered with the lysosomotropic agent chloroquine on a daily basis for 5 d prior to microscopy,[19] which may block vesicular acidification at the endosomal[20] or autolysosomal level.[21,22]

Figure 1A-D shows representative BGT-AF647 signals with pretzel-shaped NMJs (one NMJ in each panel) and their surroundings. Since CHRN density at the postsynaptic membrane is about 10,000 receptors per μm^2, with a decreasing density outside the synapse by factors of up to 1000- fold,[23,24] CHRN signals in vesicles were much weaker than those in the synapse. Thus, to display the vesicles containing endocytosed CHRN along with their corresponding NMJs, post-acquisition contrast enhancement was used, similar to previous studies of this and other laboratories.[16,18,25,26] Quantitative analysis revealed that denervation alone led to more than an 8-fold increase in the internalized CHRN vesicle number (Fig. 1A-B and E). Chloroquine treatment seemingly blocked the processing of these vesicles and led to their significant enrichment in innervated as well as denervated muscles by a factor of 2–3 when compared to the same condition in the absence of chloroquine (Fig. 1C-E). The accumulation of CHRN carriers upon chloroquine treatment of innervated muscles indicates the degradative processing of CHRN under basal conditions. Furthermore, the increase of these carriers upon denervation and in the presence of chloroquine treatment suggests that the endocytic and/or autophagic flux of CHRN has the ability to adapt to impaired neuromuscular activity.

The ratio of SH3GLB1:p-SH3GLB1 is increased upon sciatic denervation in skeletal muscles

Phosphorylation of SH3GLB1 at position T145 was previously linked to the induction of autophagy in neurons.[12] Using a primary antibody specific for phosphorylated SH3GLB1 at position T145 (from here onwards p-SH3GLB1) (Fig. S1), we tested the effect of denervation using western blot analysis. While the total amount of SH3GLB1 was upregulated in muscle lysates
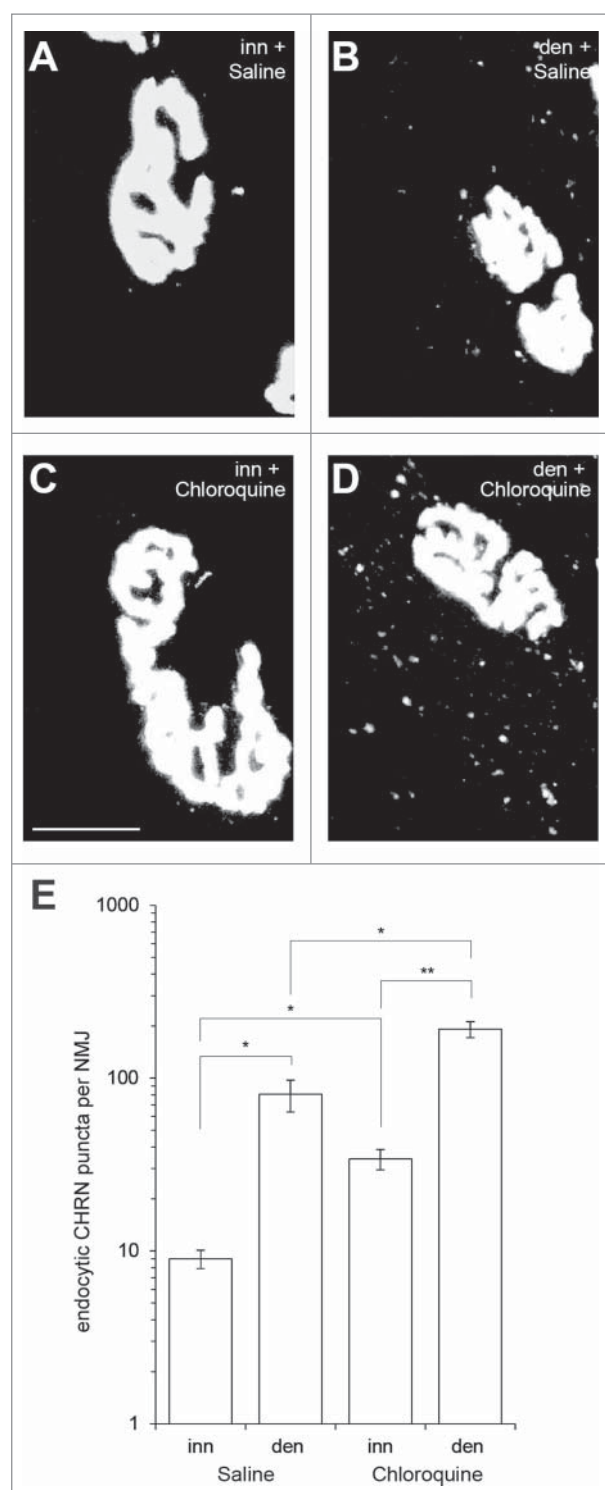
Figure 1. Denervation induces accumulation of endocytic CHRN vesicles that is further augmented in the presence of chloroquine. TA muscles from innervated (inn) and 4-d denervated (den) legs were injected with BGT-AF647 to stain surface-exposed CHRN. One d later, muscles were imaged *in situ* using confocal microscopy to observe surface-exposed (on NMJs, large pretzel-like structures) and endocytosed (on vesicles, small puncta) CHRNs. Animals were either treated with saline or chloroquine for 5 d prior to imaging. (A-D) Representative maximum-z projections displaying individual NMJs and their corresponding internalized CHRN vesicles. Scale bar: 20 μm. (E) Quantification of CHRN puncta per NMJ. Given is mean ± SEM (n = 3 muscles for each condition; * P< 0.05; ** P < 0.01; a total of 8874 puncta was analyzed). Statistical significance was probed using ANOVA.

upon denervation and chloroquine treatment, levels of p-SH3GLB1 remained constant (Fig. 2A), thus leading to a
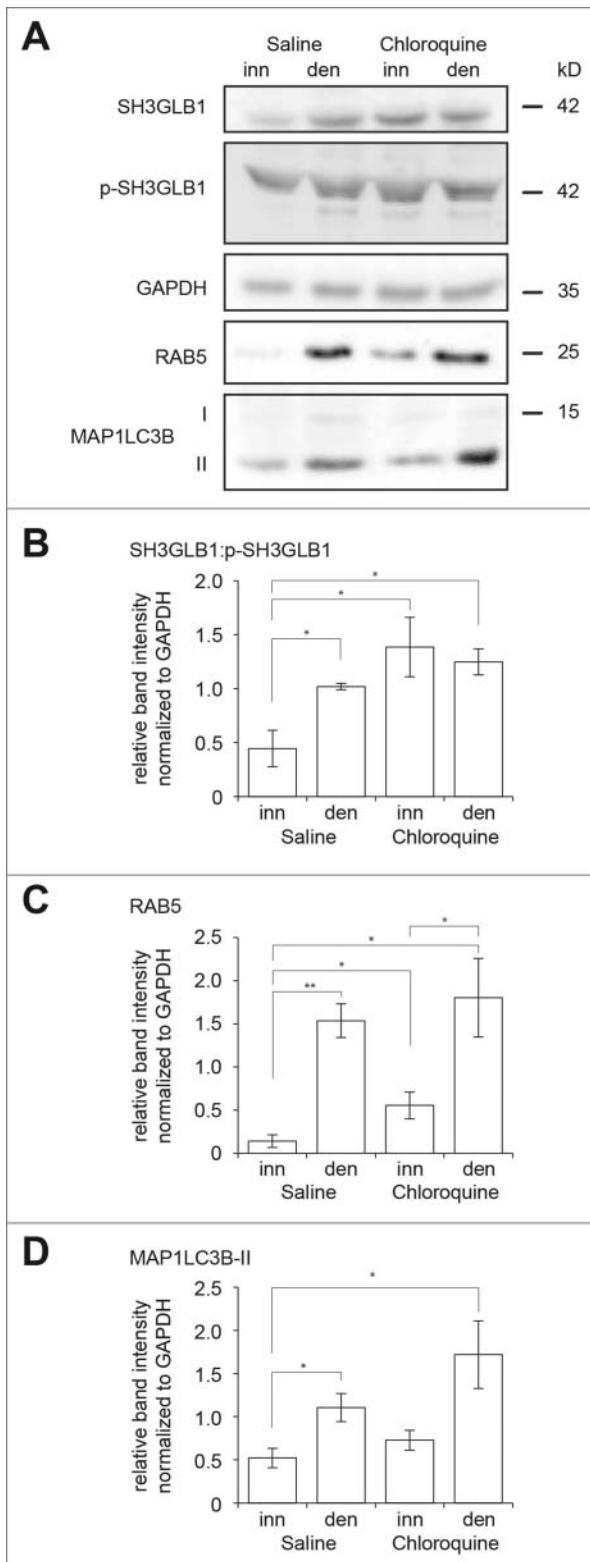
Figure 2. Denervation or chloroquine augment the ratio of total SH3GLB1 to T145-phosphorylated SH3GLB1 as well as levels of RAB5. Mice were unilaterally denervated and daily injected with saline or chloroquine for 5 d. TA muscles from innervated (inn) and denervated (den) legs were then homogenized and equal amounts of protein subjected to western blot. (A) Displayed is a representative blot showing the relative amounts of total SH3GLB1, SH3GLB1 phosphorylated at position T145 (p-SH3GLB1), RAB5, and MAP1LC3B. GAPDH served as the loading control. (B-D) Quantitative analysis of the relative band intensities for SH3GLB1:p-SH3GLB1 ratio (B), RAB5 (C), and MAP1LC3B-II (D). All values were normalized to the internal GAPDH loading controls. Shown are mean ± SEM of values obtained from 3 independent experiments. Statistical significance was probed using ANOVA, * $P < 0.05$; ** $P < 0.01$.

significantly increased proportion of the total amount of SH3GLB1 relative to p-SH3GLB1 (SH3GLB1:p-SH3GLB1) under these conditions (Fig. 2B). These results suggest that SH3GLB1:p-SH3GLB1 is precisely controlled, with data on the increase of the SH3GLB1:p-SH3GLB1 ratio upon denervation and chloroquine treatment being consistent with the involvement of SH3GLB1 phosphorylation in endosomal processing or autophagy induction. Previously, CDK5 was described to be relevant for the activity-dependent phosphorylation of SH3GLB1 and its effects on autophagy in neurons.[12] To verify if the observed activities of this kinase also correlate with SH3GLB1 phosphorylation in skeletal muscle, we addressed the abundance of CHRN vesicles and the ratio of SH3GLB1:p-SH3GLB1 in the presence of a dominant-negative form of CDK5 (CDK5 DN) in innervated versus denervated legs. As depicted in Fig. S2, the differences in CHRN vesicle numbers (Fig. S2A-B) and SH3GLB1:p-SH3GLB1 ratio (Fig. S2C-D) between the innervated and denervated conditions observed in wild-type muscles (see Figs. 1 and 2) were completely abolished in the presence of CDK5 DN. This strongly suggests that CDK5 plays a major role in the activity-dependent phosphorylation of SH3GLB1 and its effects on the trafficking of CHRN, and thus confirms the earlier data on protein trafficking in neurons. Reasons for the persistent p-SH3GLB1 band observed in the presence of CDK5 DN (Fig. S2C) may either be the signals coming from fibers not expressing the CDK5 DN construct or the presence of a basal level of phosphorylation by other kinases.

Next, we investigated the amount of markers for endosomal (RAB5) and autophagosomal compartments (MAP1LC3B-II) both in the presence and absence of innervation and chloroquine. Both markers showed comparable profiles with a significant enrichment upon denervation and in the presence of chloroquine (Fig. 2C-D), although these changes were more consistent and pronounced for RAB5. This suggests chloroquine blocks endosomal maturation as well as autophagic processing in skeletal muscle, at least under the experimental profile used here. Colocalization analysis of CHRN puncta with overexpressed GFP-MAP1LC3B (Fig. S3) and immunostained endogenous MAP1LC3B (Fig. S4) confirmed this assumption and, indeed, steady-state colocalization between these markers in the absence of chloroquine was approximately 30% and did not change upon chloroquine treatment.

Phosphomutants of SH3GLB1 modulate the processing of internalized CHRN

To address the function of SH3GLB1 phosphorylation at T145 on CHRN trafficking in more detail, we cloned phospho-deficient (T145A) and phospho-mimetic (T145E) mutants of SH3GLB1 that were coupled with mCherry fluorescent protein and tested their effects on CHRN internalization under basal, innervated conditions. T145A and T145E mutants were transfected into TA muscles. Nine d later, CHRN were labeled with BGT-AF647. Then after 24 h, the muscles were imaged with in vivo confocal microscopy. Figure 3A depicts representative fields of view. As in Figure 1, post-acquisition contrast enhancement was used to show CHRN-positive vesicles next to their corresponding NMJs. To give an idea of the actual image
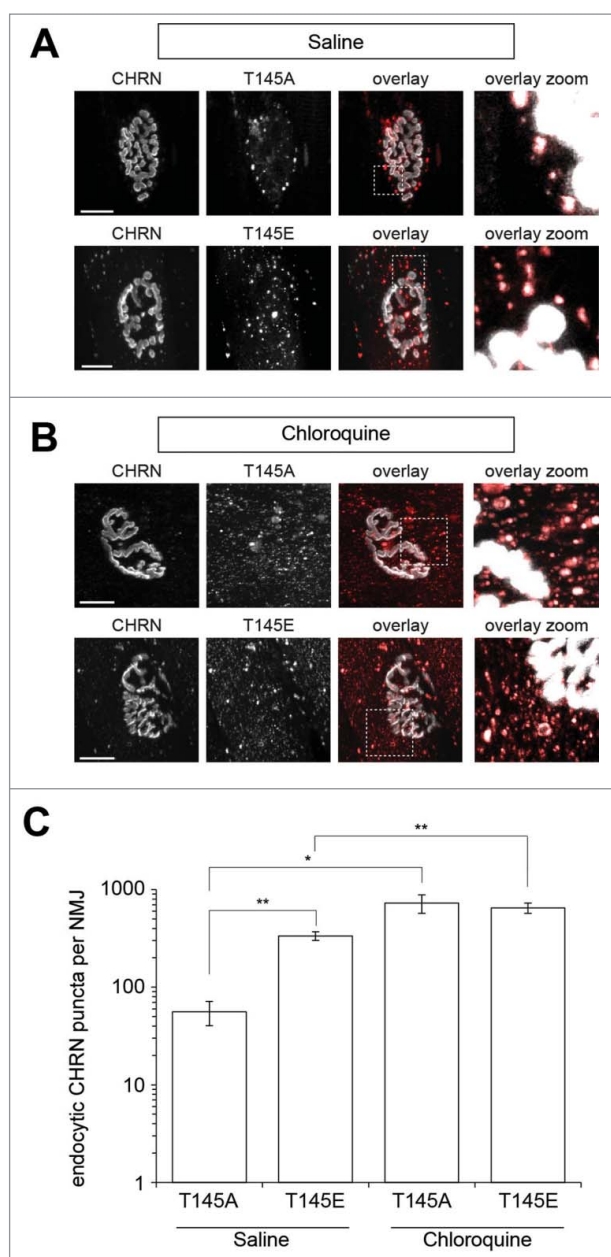
Figure 3. The number of internalized CHRN puncta is differently affected by phosphomutants of SH3GLB1 but not in the presence of chloroquine. TA muscles were transfected as indicated with SH3GLB1^T145A or SH3GLB1^T145E mutants fused with mCherry. After 9 d, CHRN were labeled using BGT-AF647. Another day later, muscles were imaged with confocal in vivo microscopy. During the 5 d before microscopy, mice either received saline (A) or chloroquine (B). (A-B) Three left panel columns show maximum-z projections of representative fluorescence signals of BGT-AF647 (CHRN), SH3GLB1 phosphomutants fused with mCherry (T145A or T145E), and overlays of both (overlay). The right panel column depicts zoom images of single optical layers of the boxed regions in the overlay images. CHRN panels are shown without contrast enhancement. Overlay zoom panels were contrast enhanced to better visualize CHRN-positive vesicles. In overlay and overlay zoom panels BGT-AF647 and mCherry signals are displayed in white/gray and red, respectively. Scale bars: 20 μm. (C) Quantitative analysis of CHRN puncta per NMJ. Shown are mean $\pm$ SEM (n = 3 muscles for each condition without chloroquine, n = 4 muscles for T145A + chloroquine, n = 6 muscles for T145E + chloroquine; Statistical significance was probed using ANOVA; * P < 0.05, ** P < 0.01; a total of 33,443 puncta was analyzed).

quality, the overview images (labeled "CHRN") are shown in all following figures without contrast enhancement, while the zoom panels were contrast enhanced. In addition, Video S1 depicts an exemplary image stack to illustrate the CHRN

channel contrast enhancement. BGT-AF647-positive puncta were consistently positive with T145A or T145E (Fig. 3A, see zoomed overlays), but the number of such CHRN-containing puncta was roughly increased 6-fold in the presence of T145E as compared to T145A (Fig. 3C). Under the same conditions, the colocalization of endogenous MAP1LC3B with CHRN-positive puncta was only slightly increased (Fig. S4), suggesting the surplus of CHRN vesicles imposed by T145E was largely not of autophagosomal nature.

Chloroquine blunts the effects of SH3GLB1 phosphomutants on the accumulation of internalized CHRN

The increase of CHRN-carrying puncta in the presence of T145E (Fig. 3C) could either be the result of augmented CHRN internalization or a kinetic modulation of the processing of CHRN endosomes by T145 phosphorylation. To test the effect of T145A and T145E on the basal endocytosis rate of CHRN, TA muscles were transfected with either T145A or T145E and received chloroquine on a daily basis for the 5 d before microscopy. Muscles were imaged in vivo 10 d after transfection and 24 h after marking CHRN with BGT-AF647. Notably, chloroquine treatment led to a significant accumulation of internalized CHRN vesicles (Fig. 3B) and blunted the differences in vesicle numbers between T145A and T145E mutants (Fig. 3C): In the absence of chloroquine, T145A and T145E transfections yielded 56 $\pm$ 16 (mean $\pm$ SEM, n = 3 muscles) and 336 $\pm$ 34 (mean $\pm$ SEM, n = 3 muscles) vesicles per field, respectively; in the presence of chloroquine, these numbers were 728 $\pm$ 156 (mean $\pm$ SEM, n = 4 muscles) and 649 $\pm$ 79 (mean $\pm$ SEM, n = 6 muscles) vesicles per field for T145A and T145E, respectively. This finding strongly suggests that the T145 phosphorylation status is not affecting endocytic CHRN carrier formation but is rather critical for endocytic or autophagic processing of CHRN. Upon chloroquine treatment, the colocalization between MAP1LC3B and CHRN-positive puncta increased only mildly, from 39 $\pm$ 12% (mean $\pm$ SEM, n = 3 muscles) to 52 $\pm$ 2% (mean $\pm$ SEM, n = 3 muscles) in the presence of T145A and from 47 $\pm$ 2% (mean $\pm$ SEM, n = 3 muscles) to 50 $\pm$ 8% (mean $\pm$ SEM, n = 3 muscles) in the presence of T145E (Fig. S4). Thus, it is unlikely chloroquine primarily blocked internalized CHRNs at the autophagosomal level in the present paradigm. To further dissect the genesis of the observed effects at the early endosomal or amphisomal level of CHRN trafficking, additional experiments were performed as described below.

RAB5 is present on endocytic CHRN carriers

We next asked if endocytosed CHRN employ the standard early endocytic regulator RAB5. Therefore, muscles were transfected with RAB5-GFP. Ten d later, BGT-AF647 was applied to mark CHRN, which was followed by in vivo imaging of these muscles. This showed point-to-point colocalization of BGT-positive puncta with RAB5-GFP (Fig. 4A). The interaction of RAB5 with CHRN-containing membranes was further substantiated using a previously established affinity co-sedimentation protocol.[27] Briefly, surface-exposed CHRN were labeled by in
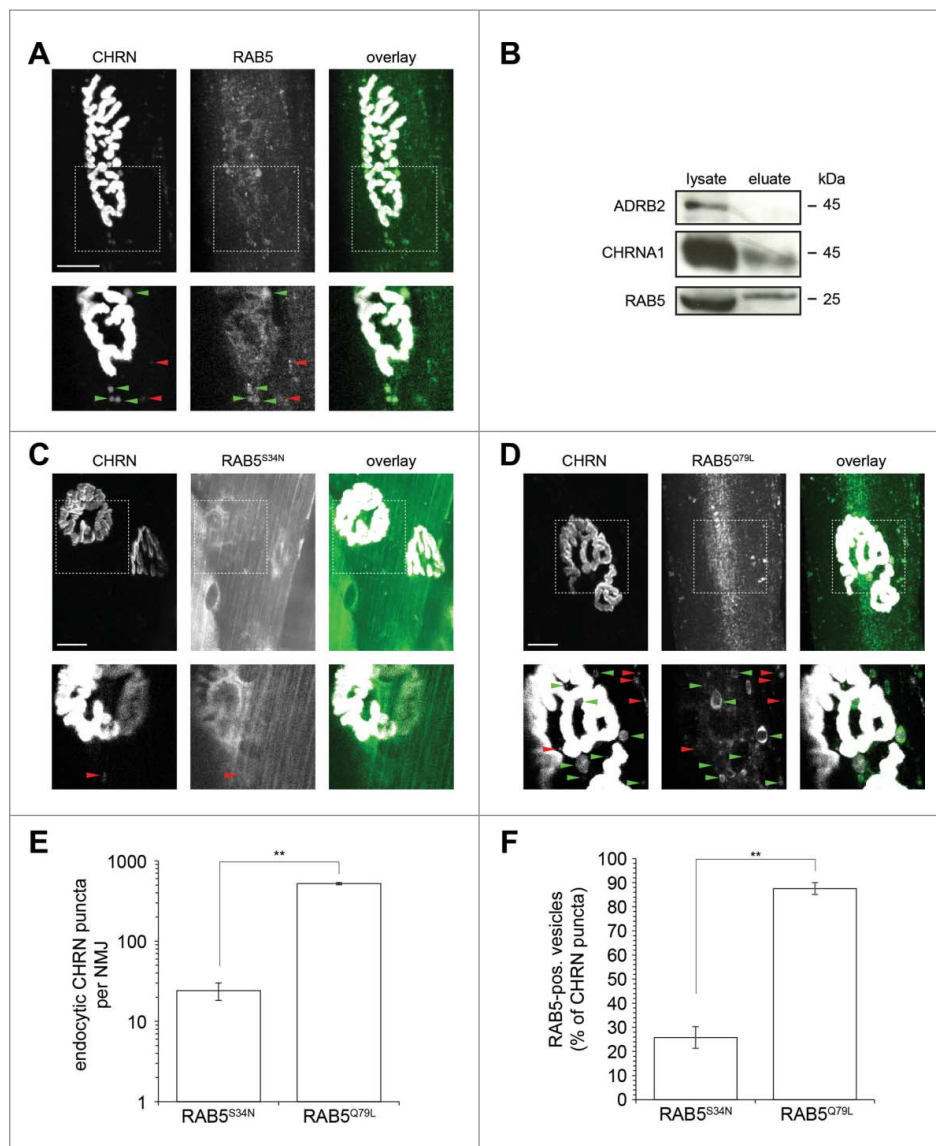
Figure 4. CHRN interacts with RAB5, and CHRN endocytosis is a RAB5-dependent process. (A) TA muscles were transfected with RAB5-GFP. After 10 d, CHRN were labeled using BGT-AF647. Confocal in vivo microscopy commenced 1 h later. Upper panels depict maximum-z projections of representative fluorescence signals of BGT-AF647 (CHRN), RAB5-GFP (RAB5), and overlays of both (overlay). Lower panels show a detail of a single optical slice of the boxed region in the upper panels focusing on puncta positive for internalized CHRN and RAB5-GFP. In overlay panels, BGT-AF647 and RAB5-GFP signals are displayed in white/gray and green, respectively. Green and red arrowheads indicate CHRN puncta colocalizing or not colocalizing with RAB5-GFP, respectively. To better visualize CHRN-positive vesicles, zoom panels were contrast enhanced. Scale bar: 20 μm. (B) Untransfected gastrocnemius muscles were injected with BGT-biotin. Five h later, muscles were harvested, homogenized and CHRN affinity precipitated with Neutravidin beads. Western blot signals upon exposure to primary antibodies against ADRB2 (negative control), RAB5, and CHRNA1 are shown. (C-E) TA muscles were transfected with RAB5 mutants S34N (C) or Q79L (D), both fused to GFP. Nine days later, CHRN were labeled using BGT-AF647. Twenty-four h later, confocal in vivo microscopy was performed. Upper panels depict maximum-z projections of representative fluorescence signals of BGT-AF647 (CHRN), RAB5 mutants fused to GFP (RAB5^{S34N} and RAB5^{Q79L}), and overlays of both (overlay). Lower panels show details of single optical slices of the boxed regions in the upper panels. In overlay panels, BGT-AF647 and GFP signals are displayed in white/gray and green, respectively. Green and red arrowheads indicate CHRN puncta colocalizing or not colocalizing with RAB5-GFP, respectively. To better visualize CHRN-positive vesicles, zoom and overlay panels were contrast enhanced. Scale bar: 20 μm. (E-F) Quantitative analysis of the number (E) and colocalization with GFP signals (F) of CHRN-positive puncta. Depicted are mean $\pm$ SEM (n = 5 muscles for RAB5^{S34N}, n = 3 muscles for RAB5^{Q79L}; statistical analysis employed ANOVA; ** P < 0.01).

vivo injection of biotin-conjugated BGT. After allowing endocytosis of marked CHRN for 5 h, muscles were then harvested and a standard neutravidin-bead precipitation was performed, followed by a SDS-PAGE and western blot. Co-sedimentation of RAB5 protein with CHRN, corroborating the immuno-staining and in vivo imaging data, revealed that RAB5 is present in an endocytic CHRN molecular complex (Fig. 4B).

Finally, we studied the functional relevance of RAB5 for CHRN endocytosis by means of the RAB5 mutants Q79L and S34N.[28] Following the classical Rab cycle scheme, the binding of membrane-attached RAB5 to either GTP or GDP mediates the active and inactive states of the GTPase, respectively. While RAB5^{S34N} has high GTPase activity and, thus, is mostly in an inactive state, the inverse is true for the RAB5^{Q79L} mutant.[28] In cultured cells, inhibition of endocytosis or accumulation of large-sized endosomes are observed in the presence of either RAB5^{S34N} or RAB5^{Q79L}, respectively.[28] In accordance with these earlier studies, we found clear differences in CHRN vesicle numbers between RAB5^{S34N}- and RAB5^{Q79L}-expressing muscles. Figure 4C-D show

representative in vivo images of NMJs of TA muscles transfected with RAB5^{S34N} (Fig. 4C) or RAB5^{Q79L} (Fig. 4D). Whereas the first exhibited only 24 ± 6 CHRN-positive puncta per NMJ (mean ± SEM, n = 5 muscles), RAB5^{Q79L} expression led to a strong increase in the amount of endocytic carriers (520 ± 17, mean ± SEM, n = 3 muscles, Fig. 4E). Also, whereas RAB5^{S34N} showed more or less an even distribution and colocalized with only 26 ± 5% (mean ± SEM, n = 5 muscles, Fig. 4F) of CHRN puncta, RAB5^{Q79L} had a more punctate distribution pattern, often induced very large vesicular structures, and colocalized with 88 ± 2% (mean ± SEM, n = 3 muscles, Fig. 4F) of CHRN signals. In summary, these data demonstrate that RAB5 is crucial for CHRN endocytosis and further processing.

Overexpression of RAB5-GFP strongly reduces the amount of internalized CHRN in the presence of T145E SH3GLB1

To address if the early endosomal processing could be affected in the presence of SH3GLB1 phosphomutants, we analyzed CHRN vesicle numbers in the presence of SH3GLB1 phosphomutants while simultaneously overexpressing RAB5-GFP. TA muscles were cotransfected with the corresponding cDNAs and injected 9 d later with BGT-AF647. Twenty-four h thereafter, muscles were imaged with in vivo confocal microscopy (Fig. 5A-B). In particular, this analysis showed a highly significant reduction (P < 0.01) in CHRN vesicle numbers from 336 ± 34 (mean ± SEM, n = 4 muscles, see Fig. 3C) to 107 ± 19 (mean ± SEM, n = 8 muscles, Fig. 5E) for T145E-transfected muscles in the absence or presence of RAB5-GFP, respectively. Conversely, RAB5-GFP overexpression had no significant effect on CHRN vesicle numbers in T145A-expressing muscles. Colocalization of BGT-positive puncta with RAB5-GFP was very similar upon co-expression of either T145A (31 ± 4%, mean ± SEM, n = 11 muscles) or T145E (35 ± 6%, mean ± SEM, n = 8 muscles) (Fig. 5F). The effects of RAB5-GFP on the abundance of CHRN puncta were most likely not due to homotypic fusion by overexpressed RAB5 protein for the following 2 reasons: First, although RAB5-GFP expression levels were often very different from fiber to fiber (Fig. S5A), CHRN vesicle numbers did not vary between fibers expressing high or low amounts of RAB5-GFP (Fig. S5B).
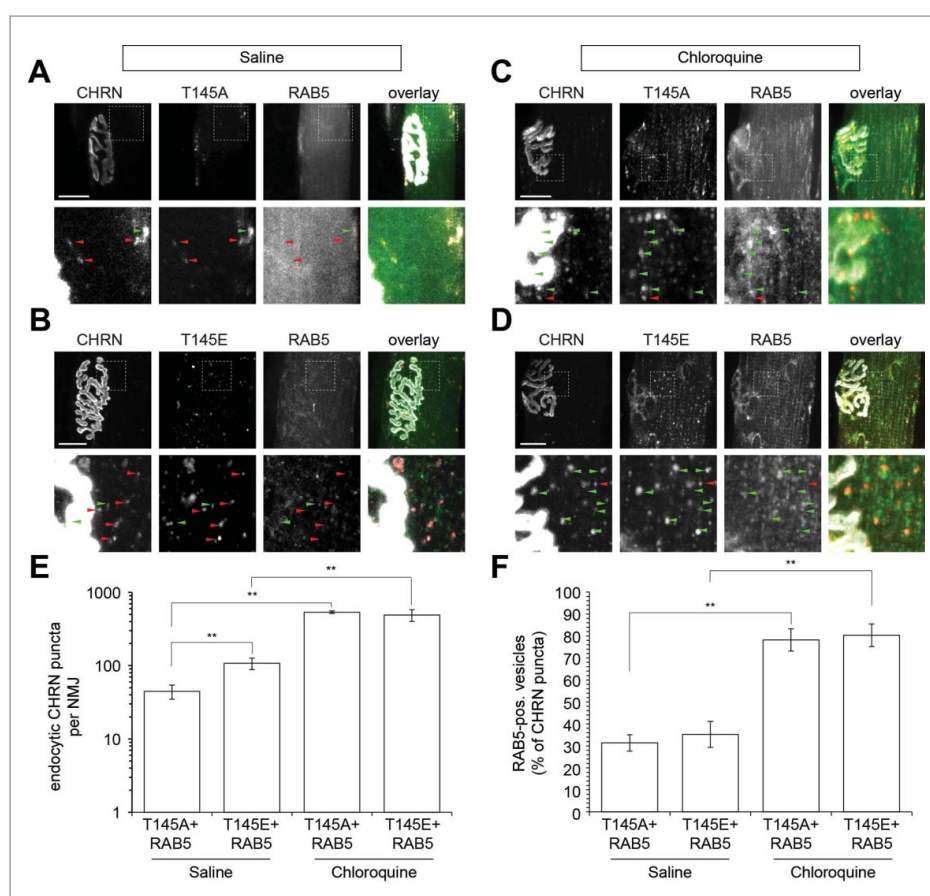
Figure 5. Overexpression of RAB5-GFP reduces the number of internalized CHRN puncta in the presence of T145E in a chloroquine-dependent manner. TA muscles were cotransfected with RAB5-GFP and SH3GLB1^{T145A} (A and C) or SH3GLB1^{T145E} (B and D) mutants coupled to mCherry. Nine d after transfection, CHRN were labeled using BGT-AF647. Another day later, muscles were imaged with confocal in vivo microscopy. During the 5 d before microscopy, mice either received saline (A, B) or chloroquine (C, D). (A-D) Upper panels show representative NMJs and their CHRN puncta (CHRN), mCherry (T145A or T145E), and GFP (RAB5) signals, as indicated. Lower panels depict details of single optical layers from the boxed regions of upper panels. In the overlay pictures, mCherry, RAB5-GFP, and CHRN signals are shown in red, green, and gray/white, respectively. CHRN, mCherry, and RAB5-GFP triple-positive puncta are indicated with green arrowheads. CHRN and mCherry puncta not positive for RAB5-GFP are indicated with red arrowheads. Scale bars: 20 μm. (E) Quantitative analysis of CHRN puncta per NMJ. Mean ± SEM (n = 11 muscles for T145A and n = 8 muscles for T145E in the absence of chloroquine; n = 4 muscles each for T145A and T145E in the presence of chloroquine; statistical analysis employed ANOVA; ** P < 0.01; a total of 38,808 puncta was analyzed). (F) Colocalization analysis of RAB5-GFP-positive CHRN puncta. Mean ± SEM (n-values as in [E]; statistical analysis employed ANOVA; ** P < 0.01).

Second, within the constraint of diffraction-limited resolution, the distribution of CHRN vesicle size was only marginally different between untransfected and T145A- or T145E-expressing muscles (Fig. S5C).

In contrast, chloroquine treatment of RAB5-GFP and T145A or T145E cotransfected muscles led to a massive increase in CHRN vesicle numbers and colocalization between CHRN vesicles and RAB5-GFP (Fig. 5C-D). As shown in Fig. 5E, RAB5-GFP+T145A and RAB5-GFP+T145E cotransfected muscles resulted in 537 ± 21 (mean ± SEM, n = 4 muscles) and 490 ± 90 (mean ± SEM, n = 4 muscles) CHRN vesicles per NMJ, respectively. Thus, both were found not to be statistically different from the corresponding T145A or T145E single-transfected muscles in the presence of chloroquine, see Fig. 3C. Colocalization between RAB5-GFP and CHRN vesicles augmented to 78 ± 5% (mean ± SEM, n = 4 muscles, Fig. 5F) for T145A-transfected muscles and 80 ± 5% (mean ± SEM, n = 4 muscles, Fig. 5F) for T145E-transfected muscles in the presence of chloroquine. These data strongly suggest a chloroquine-induced block of the degradation and progression from the early-endosomal to either late-endosomal or autophagosomal stage of CHRN vesicles. Yet, differences between T145A and T145E in terms of CHRN vesicle processing as described in Figure 3 remained unexplained because vesicular binding of RAB5 was seemingly the same in the presence of T145A or T145E.

To address the question if phosphorylation of SH3GLB1 may be important for the expression or activation cycle of RAB5, TA muscles were single transfected with either T145A or T145E, then lysed after 10 d. Western blot analysis revealed that the abundance of RAB5 protein was not influenced by SH3GLB1 phosphomutants (Fig. S6). Conversely, the amounts of 2 important regulators of RAB5 activity, RABGEF1 (RAB guanine nucleotide exchange factor 1) and USP6NL (USP6 N-terminal like), were modulated (Fig. S6). While the guanylyl exchange factor RABGEF1, which loads new GTP on membrane-bound RAB5 and thus activates its function,[29] was upregulated in the presence of both T145A and T145E, the levels of the GTPase activating protein USP6NL, which switches RAB5 from the active to the inactive conformation,[30] were decreased in the presence of T145A and variable in the presence of T145E. Together, these results indicate that the phosphorylation status of SH3GLB1 might act on CHRN endosomal processing by modulation of the RAB5 activity cycle.

Discussion

Proper neuromuscular transmission at the NMJ depends on an adequate postsynaptic density of CHRN.[31] This density is strongly regulated by the degradative trafficking of CHRN, which is a major determinant of CHRN turnover.[25,32] Because the degradative route of CHRN is particularly augmented under pathophysiological conditions, such as myasthenia gravis, congenital myasthenic syndromes, muscle atrophy, and sarcopenia,[33–35] the identification of the molecular machinery controlling CHRN endo/lysosomal trafficking is of considerable biomedical interest. We previously showed that the autophagic pathway mediates the degradation of endocytosed CHRN and that SH3GLB1 accompanies vesicles containing endocytosed CHRN.[16,36] Furthermore, the number of CHRN-positive vesicles increases upon sciatic denervation in a TRIM63-dependent manner.[16] The association of SH3GLB1 with the trafficking of transmembrane proteins, in this case CHRN, is

not only consistent with previous observations where SH3GLB1 was found to interact with other trans-membrane receptors, such as NTRK1/tyrosine receptor kinase A[37] and EGFR (epidermal growth factor receptor),[9] at the level of the early endosome but also regulates their endocytic processing and sorting. We expanded on these findings by providing novel insights into how posttranslational modifications, such as phosphorylation of SH3GLB1, might regulate endosomal trafficking.

Corroborating our previous reports, here we show the abundance of endolysosomal carriers of CHRN is increased upon an atrophic stimulus (sciatic denervation) and that degradation of these carriers can be perturbed in vivo using the lysosomotropic agent chloroquine (Fig. 1). These data fit with the observation that lysosomal inhibitors affect the degradation rate of CHRN in chicken embryo skeletal muscles.[38] Furthermore, chloroquine treatment of mice led to a significant increase of the early endosome marker RAB5 (Fig. 2) as well as a less pronounced rise of the autophagosomal marker MAP1LC3B-II (Fig. 2). Since, additionally, chloroquine did not alter colocalization of CHRN vesicles with GFP-MAP1LC3B (Fig. S3) but significantly increased colocalization of CHRN carriers with RAB5-GFP (Fig. 5C-F), these findings suggested a principal effect of chloroquine on blocking endocytosis rather than autophagy. Although chloroquine is often used to block autophagy, the literature reports a considerable variability regarding its effects on MAP1LC3B-II amounts in skeletal muscle. Some chloroquine treatment paradigms of rat and mouse models showed an increase in MAP1LC3B-II,[39–41] whereas others did not.[42,43] Mainly, an increase in MAP1LC3B-II was typically detected after weeks of treatment, suggesting that chloroquine may not necessarily, and certainly not exclusively, block degradative processing at the autophagosomal level. Consistent with chloroquine-induced endocytic abnormalities in pheochromocytoma 12 cells,[20] our observations add to the notion[44] that it is important to carefully investigate at which level of trafficking chloroquine might act in a particular treatment paradigm.

Chloroquine as well as denervation increased CHRN vesicle numbers and the SH3GLB1:p-SH3GLB1 ratio (Fig. 2), suggesting an involvement of SH3GLB1 phosphorylation in the regulation of CHRN endocytic processing. A previous study reported that phosphorylation of SH3GLB1 by the kinase CDK5 is crucial for regulating autophagic activity upon starvation in mice.[12] Consistent with this, we found that overexpression of a dominant negative CDK5 ablated both the denervation-induced increase in CHRN vesicle number as well as SH3GLB1:p-SH3GLB1 ratio (Fig. S2). To further investigate the role of SH3GLB1 phosphorylation in the context of CHRN endocytic processing, we used the overexpression of SH3GLB1 phosphomutants T145A and T145E in TA muscles and found significantly less CHRN-positive vesicles in the presence of T145A as compared to T145E (Fig. 3C). Given that the differences in CHRN vesicles between T145A- and T145E-expressing muscles were absent upon chloroquine treatment (Fig. 3C), we speculate that T145A might enhance and/or T145E might slow down endosomal processing.

Based on the finding that SH3GLB1 is important for the recruitment of RAB5 in cells[45] as well as our observation of similar abundance profiles for CHRN vesicles (Fig. 1) and RAB5 proteins (Fig. 2) in live muscle tissue we tested the hypothesis that while CHRN endocytosis might depend on RAB5, the recruitment,

abundance or activity of RAB5 might be regulated by SH3GLB1 phosphorylation. As already mentioned, our data show that RAB5[28] accompanies endocytosed CHRN in skeletal muscles in vivo (Fig. 4). Furthermore, the number of CHRN vesicles and their colocalization with RAB5 appeared to be strongly dependent on the activity of RAB5 because the overexpression of GTPase hyperactive and hypoactive mutants altered both parameters very strongly (Fig. 4D-F). Fitting with earlier reports that RAB5 overexpression can accelerate maturation of cargo-containing phagosomes,[46] co-expression of RAB5 with T145E largely rescued the slow processing of CHRN endosomes (Fig. 5B and E). These findings would argue that either the recruitment or abundance of RAB5 may be regulated by SH3GLB1 phosphorylation status, but both characteristics were unaltered between the different conditions (Fig. 5F and Fig. S6). However, different amounts of RAB5 activity-modifying enzymes in the absence or presence of T145A and T145E could be detected (Fig. S6), suggesting SH3GLB1 might modulate the activity-cycle of RAB5 and, thereby, control CHRN endocytic processing. However, further investigations need to address this point.

Altogether, our data indicate that muscle atrophic stimuli enhance endocytosis of CHRNs, and their proper endosomal/autophagic processing critically depends on SH3GLB1 phosphorylation. As previously shown,[16,18] the degradation of CHRN upon endocytosis in atrophic conditions is tightly regulated by the atrogene and E3 ubiquitin ligase, TRIM63.[47] Thus, it would be interesting to investigate if the levels of SH3GLB1:p-SH3GLB1 are also modulated in an atrogene-dependent manner. In summary, using live skeletal muscle imaging and biochemical analysis, we have shown that the number of CHRN endosomes is increased upon sciatic denervation. These CHRN-containing carriers are accompanied by differentially T145-phosphorylated SH3GLB1, with this phosphorylation status regulating the rate of CHRN endosomal processing by acting on RAB5 function.

Materials and methods

Animals, transfection and sciatic denervation

In the current study, adult C57BL/10J mice were used. Animals were maintained in a local animal facility. Use and care of these animals were as approved by German authorities and according to national law (TierSchG7). For anesthesia either an intraperitoneal injection of Xylavet® 20 mg/ml (cp-pharma) and Zoletil® 100 (Laboratoires Virbac) or inhalation of Isofluran (cp-pharma, AP/DRUGS/220/96) was used. Transfection of the respective cDNA was performed by intramuscular injection of plasmid DNA (10 μg) in the TA muscle, followed by electroporation as described previously.[48] In all experimental conditions, the left hindlimb was denervated and the contralateral right side served as the control. For sciatic denervation approximately 5 mm of the sciatic nerve was removed.[34] Regeneration of the sciatic nerve was checked after the experiments were completed.

Chloroquine treatment, western blot and affinity cosedimentation

Animals were administered 25 mg/kg chloroquine (Sigma-Aldrich, C6628) in PBS (137 mM NaCl, 2.7 mM KCl, 10 mM Na$_2$HPO$_4$ x 2

H$_2$O, 2 mM KH$_2$PO$_4$, pH 7.4) intraperitoneally for 5 d prior to experimental analysis, with PBS injected animals acting as the control. For western blot analysis, either transfected TA muscles or gastrocnemius muscles from chloroquine- and PBS-treated animals were harvested immediately after animal sacrifice, shock frozen in liquid nitrogen and stored at −80°C. Frozen tissues were then homogenized in 1 mL IP lysis buffer (50 mM Tris-HCl, pH 8.0, 150 mM NaCl, 1% NP-40 [AppliChem, A1694], 10% glycerol, 1 mM EDTA, 1 mM EGTA, Roche® phosphatase inhibitor cocktail [1x; 88667], Roche® protease inhibitor cocktail [1x; 88665] and 0.5 mM PMSF [AppliChem, A0999]). Next, to get rid of the tissue debris, homogenates were centrifuged for 10 min. Protein concentration of the homogenate was measured using the Bradford assay. Subsequently, homogenate containing approximately 50 μg of protein in Laemmli buffer was loaded on a 12% polyacrylamide gel. Next, proteins were transferred to PVDF membranes. For validating the specificity of anti p-T145 SH3GLB1 antibody, dot blots (Fig. S1) of muscle lysates were performed. Therefore, muscles were homogenized in 1 mL IP lysis buffer lacking Roche® phosphatase inhibitor cocktail and incubated with shrimp alkaline phosphatase (New England Biolabs, M0371S) overnight at 37°C, untreated lysate was used as the control. Lysate dots were applied on PVDF membrane followed by immunodetection. For affinity coprecipitation (Fig. 4B) gastrocnemius muscles were injected with 125 pmoles of BGT coupled with biotin (Invitrogen, B1196) and then harvested after 5 h. Tissue lysis was performed as mentioned above, while affinity precipitation with NeutrAvidin beads (Thermo Fisher Scientific, 29202) and western blot were performed as previously described.[27,49] The following antibodies were used for the detection of their respective proteins: mouse anti-SH3GLB1 (Imgenex, IMG-265A), guinea pig anti-phospho-SH3GLB1 custom made with synthetic peptide (NFLpTPLRNFIC, PSL), rabbit anti-RAB5 (Cell Signalling Technology, 3547), mouse anti-GAPDH/glyceraldehyde-3-phosphate dehydrogenase (Thermo Fisher Scientific, MA5-15738), rabbit anti-ADRB2/adrenoceptor β 2 (Santa Cruz Biotechnology, sc-569), mouse anti-CHRN (BD Bioscience, 610989), rabbit anti-MAP1LC3B (Genetex, GTX127375), Living Colors® A.v. monoclonal antibody JL-8 (Clontech Laboratories, 632380), anti-mCherry (Acris, AP32117 PU), anti-USP6NL (Bethyl Laboratories, A302-794A-M), anti-RABGEF1 (Cell Signalling Technology, 7622), anti-rabbit coupled to horseradish peroxidase (HRP; Dako, P0448), anti-mouse-HRP (Thermo Fisher Scientific, 32430), anti-guinea pig-HRP (Thermo Fisher Scientific, PA1-28597), anti goat-HRP (Dako, P0449). Chemiluminescence signals were obtained using a chemiluminescence imager (G:Box Chemi XX6, Syngene; Fig. 2, Fig. S1, and Fig. S6), or exposure to Hyperfilm ECL (Amersham, 95017-659; Fig. 4B).

Immunostaining

Transfected and untransfected TA muscles were treated with either saline or 25 mg/kg chloroquine for 5 d. Muscles were harvested, chemically fixed overnight at 4°C in 4% wt/vol paraformaldehyde in PBS and embedded in 2% agarose (AppliChem, A8963). A vibratome (Leica Biosystems, Nussloch, Germany, VT1000S) was used for preparing 40-μm-thick longitudinal muscle sections. These sections were then quenched with 0.3 M glycine in PBS, permeabilized with 0.5% Triton X-100 (Roth, 3051.4) in PBS, blocked with 3% BSA (Roth, 3737.2) in PBS, and stained with rabbit anti-

MAP1LC3B, followed by BGT-AF647 (Life Technologies, B35450) and donkey anti-rabbit Alexa Fluor 488 (Invitrogen, A21206). Last, slices were washed, placed on a slide and embedded in Mowiol (Roth, 0713.2) for confocal microscopy.

Expression plasmids

For in vivo transfection of mice TA muscles, the following constructs encoding heterologous fusion proteins were used: RAB5-GFP (kindly provided by Dr. Walter Volknandt, Frankfurt, Germany), pcDNA3-dnCDK5 as a gift from Li-Huei Tsai (Addgene, 1344), pTagRFP-N (Evrogen, FP142), pcDNA 3.1 (kindly provided by Dr. Olivier Kassel, Karlsruhe, Germany), pEGFP-MAP1LC3B (kindly provided by Dr. Marco Sandri, Padua, Italy), EGFP-Rab5A Q79L and EGFP-Rab5A S34N as gifts from Dr. Qing Zhong (Addgene, 28046 and 28045). SH3GLB1 phosphomutants were cloned into pmCherry vector backbone (Clontech Laboratories, 632522). Here, the threonine 145 amino acid residue was mutated to alanine (SH3GLB1^{T145A}) or glutamic acid (SH3GLB1^{T145E}) using an overlapping PCR mutagenesis technique. Tests for the usefulness of the expression constructs were performed (Fig. S7), which involved comparisons to empty mCherry vectors and to SH3GLB1 fusion constructs with other plasmids. Therefore, the following vectors and fusion constructs were employed: pcDNA3.1, ptagRFP1, pmCherry-SH3GLB1, and ptagRFP1-SH3GLB1.

Microscopy

Twenty-four h before in vivo confocal microscopy, muscles were injected with 31 pmoles of BGT-AF647. In the case of transfected muscles, in vivo microscopy was performed 10 d after transfection. Animals were anesthetized and images of TA muscles were taken with an upright Leica SP2 (Leica Microsystems, Mannheim, Germany) confocal microscope equipped with a 63 ×/1.2 NA water immersion objective. 3D stacks were taken at 8-bit, 1024 pixel resolution, 200 Hz scan frequency, and at an electronic zoom of 2.

Image analysis

Images were electronically processed using ImageJ software (NIH, Bethesda, MD). The quantitative analysis of vesicle numbers and colocalization was performed as described previously.[16] First, image stacks had the background subtracted. Then, screening of CHRN and T145A- or T145E-mCherry signals yielded total amounts of CHRN- and SH3GLB1-positive structures, which were imported into a region of interest manager. Finally, these segments were screened in all channels for colocalization. In Figure 1, only CHRN-positive puncta were counted. For Figure S5C, the areas of CHRN-positive regions of interest were measured. For western blot analysis, densities of bands were quantified using the Gel Analysis plugin of ImageJ software. Relative values were then normalized to the housekeeping gene (*GAPDH*). Images were composed using Adobe Illustrator (Adobe Systems Software) and ImageJ. All numeric data were handled using Microsoft Excel 2010 and were subsequently incorporated into the Adobe Illustrator composite. Significance was tested using the Student *t* test whenever it was applicable. Kolmogorov-Smirnow-test and ANOVA F-test were performed for checking normal distribution and homo/heteroscedasticity, respectively. The various significance levels are indicated in all respective figures.

Abbreviations

ADRB2	adrenoceptor β 2
BGT	α-bungarotoxin
BGT-AF647	BGT coupled to Alexa Fluor 647
CDK5	cyclin dependent kinase 5
CDK5 DN	dominant negative CDK5 with aspartic acid at residue 144 mutated to asparagine
CHRN/AChR	cholinergic receptor nicotinic
den	denervated
GAPDH	glyceraldehyde-3-phosphate dehydrogenase
GFP	green fluorescent protein
HRP	horseradish peroxidase
inn	innervated
MAP1LC3B	microtubule-associated protein 1 light chain 3 β
NMJ	neuromuscular junction
RAB5	member RAS oncogene family
RAB5^{Q79L}	RAB5 with glutamine at residue 79 mutated to lysine
RAB5^{S34N}	RAB5 with serine at residue 34 mutated to asparagine
RABGEF1/RABEX5	RAB guanine nucleotide exchange factor 1
SEM	standard error of the mean
SH3GLB1/Bif-1/endophilin B1	SH3 domain containing GRB2 like endophilin B1
p-SH3GLB1	SH3GLB1 phosphorylated at residue threonine 145
TA	tibialis anterior
T145A	SH3GLB1 with threonine at residue 145 mutated to alanine
T145E	SH3GLB1 with threonine at residue 145 mutated to glutamic acid
TRIM63/MURF1	tripartite motif containing 63
v-ATPase	vacuolar-type H$^+$-ATPase
USP6NL/RN-tre	USP6 N-terminal like

Disclosure of potential conflicts of interest

No potential conflicts of interest were disclosed.

Acknowledgments

Funding

ORCID

Muzamil Majid Khan (ID) http://orcid.org/0000-0002-8188-0251
Rüdiger Rudolf (ID) http://orcid.org/0000-0002-0833-1053

References

[1] Klionsky DJ, Eskelinen E-L, Deretic V. Autophagosomes, phagosomes, autolysosomes, phagolysosomes, autophagolysosomes… wait, I'm confused. Autophagy 2014; 10:549-51; PMID:24657946; http://dx.doi.org/10.4161/auto.28448

[2] Gordon PB, Seglen PO. Prelysosomal convergence of autophagic and endocytic pathways. Biochem Biophys Res Commun 1988; 151:40-7; PMID:3126737; http://dx.doi.org/10.1016/0006-291X(88)90556-6

[3] Mizushima N, Yoshimori T, Ohsumi Y. The role of Atg proteins in autophagosome formation. Annu Rev Cell Dev Biol 2011; 27:107-32; PMID:21801009; http://dx.doi.org/10.1146/annurev-cellbio-092910-154005

[4] Suzuki K, Kirisako T, Kamada Y, Mizushima N, Noda T, Ohsumi Y. The pre-autophagosomal structure organized by concerted functions of APG genes is essential for autophagosome formation. EMBO J 2001; 20:5971-81; PMID:11689437; http://dx.doi.org/10.1093/emboj/20.21.5971

[5] Lamb CA, Yoshimori T, Tooze SA. The autophagosome: origins unknown, biogenesis complex. Nat Rev Mol Cell Biol 2013; 14:759-74; PMID:24201109; http://dx.doi.org/10.1038/nrm3696

[6] Takahashi Y, Meyerkord CL, Wang HG. Bif-1/endophilin B1: a candidate for crescent driving force in autophagy. Cell Death Differ 2009; 16:947-55; PMID:19265852; http://dx.doi.org/10.1038/cdd.2009.19

[7] Takahashi Y, Meyerkord CL, Hori T, Runkle K, Fox TE, Kester M, Loughran TP, Wang HG. Bif-1 regulates Atg9 trafficking by mediating the fission of Golgi membranes during autophagy. Autophagy 2011; 7:61-73; PMID:21068542; http://dx.doi.org/10.4161/auto.7.1.14015

[8] Schimmöller F, Simon I, Pfeffert SR. Rab GTPases, directors of vesicle docking. J Biol Chem 1998; 273:22161-4; PMID:9712825; http://dx.doi.org/10.1074/jbc.273.35.22161

[9] Zhang C, Li A, Zhang X, Xiao H. A novel TIP30 protein complex regulates EGF receptor signaling and endocytic degradation. J Biol Chem 2011; 286:9373-81; PMID:21252234; http://dx.doi.org/10.1074/jbc.M110.207720

[10] Clague MJ, Urbé S, Aniento F, Gruenberg J. Vacuolar ATPase activity is required for endosomal carrier vesicle formation. J Biol Chem 1994; 269:21-4; PMID:8276796

[11] Zhang C, Li A, Gao S, Zhang X, Xiao H. The TIP30 Protein Complex, Arachidonic Acid and Coenzyme A Are Required for Vesicle Membrane Fusion. PLoS One 2011; 6:e21233; PMID:21731680; http://dx.doi.org/10.1371/journal.pone.0021233

[12] Wong ASL, Lee RHK, Cheung AY, Yeung PK, Chung SK, Cheung ZH, Ip NY. Cdk5-mediated phosphorylation of endophilin B1 is required for induced autophagy in models of Parkinson's disease. Nat Cell Biol 2011; 13:568-79; PMID:21499257; http://dx.doi.org/10.1038/ncb2217

[13] Takahashi Y, Meyerkord CL, Wang HG. BARgaining membranes for autophagosome formation: Regulation of autophagy and tumorigenesis by Bif-1/Endophilin B1. Autophagy 2008; 4:121-4; PMID:18032918; http://dx.doi.org/10.4161/auto.5265

[14] Runkle KB, Meyerkord CL, Desai NV, Takahashi Y, Wang H-G. Bif-1 suppresses breast cancer cell migration by promoting EGFR endocytic degradation. Cancer Biol Ther 2014; 13:956-66; http://dx.doi.org/10.4161/cbt.20951

[15] Takahashi Y, Coppola D, Matsushita N, Cualing HD, Sun M, Sato Y, Liang C, Jung JU, Cheng JQ, Mule JJ, et al. Bif-1 interacts with Beclin 1 through UVRAG and regulates autophagy and tumorigenesis. Nat Cell Biol 2007; 9:1142-51; PMID:17891140; http://dx.doi.org/10.1038/ncb1634

[16] Khan MM, Strack S, Wild F, Hanashima A, Gasch A, Brohm K, Reischl M, Carnio S, Labeit D, Sandri M, et al. Role of autophagy, SQSTM1, SH3GLB1, and TRIM63 in the turnover of nicotinic acetylcholine receptors. Autophagy 2014; 10:123-36; PMID:24220501; http://dx.doi.org/10.4161/auto.26841

[17] Yamaguchi H, Woods NT, Dorsey JF, Takahashi Y, Gjertsen NR, Yeatman T, Wu J, Wang H-G. SRC directly phosphorylates Bif-1 and prevents its interaction with Bax and the initiation of anoikis. J Biol Chem 2008; 283:19112-8; PMID:18474606; http://dx.doi.org/10.1074/jbc.M709882200

[18] Rudolf R, Bogomolovas J, Strack S, Choi K-R, Khan MM, Wagner A, Brohm K, Hanashima A, Gasch A, Labeit D, et al. Regulation of nicotinic acetylcholine receptor turnover by MuRF1 connects muscle activity to endo/lysosomal and atrophy pathways. Age (Dordr) 2013; 35:1663-74; PMID:22956146; http://dx.doi.org/10.1007/s11357-012-9468-9

[19] Chen GL, Sutrina SL, Frayer KL, Chen WW. Effects of lysosomotropic agents on lipogenesis. Arch Biochem Biophys 1986; 245:66-75; PMID:3947102; http://dx.doi.org/10.1016/0003-9861(86)90190-6

[20] Yuyama K, Yamamoto N, Yanagisawa K. Chloroquine-induced endocytic pathway abnormalities: Cellular model of GM1 ganglioside-induced Abeta fibrillogenesis in Alzheimer's disease. FEBS Lett 2006; 580:6972-6; PMID:17161396; http://dx.doi.org/10.1016/j.febslet.2006.11.072

[21] Cain CC, Murphy RF. A chloroquine-resistant Swiss 3T3 cell line with a defect in late endocytic acidification. J Cell Biol 1988; 106:269-77; PMID:2892844; http://dx.doi.org/10.1083/jcb.106.2.269

[22] Cain CC, Murphy RF. Growth inhibition of 3T3 fibroblasts by lysosomotropic amines: correlation with effects on intravesicular pH but not vacuolation. J Cell Physiol 1986; 129:65-70; PMID:3760033; http://dx.doi.org/10.1002/jcp.1041290110

[23] Fambrough DM. Control of acetylcholine receptors in skeletal muscle. Physiol Rev 1979; 59:165-227; PMID:375254

[24] Tintignac LA, Brenner H-R, Rüegg MA. Mechanisms Regulating Neuromuscular Junction Development and Function and Causes of Muscle Wasting. Physiol Rev 2015; 95:809-52; PMID:26109340; http://dx.doi.org/10.1152/physrev.00033.2014

[25] Akaaboune M, Culican SM, Turney SG, Lichtman JW. Rapid and reversible effects of activity on acetylcholine receptor density at the neuromuscular junction in vivo. Science 1999; 286:503-7; PMID:10521340; http://dx.doi.org/10.1126/science.286.5439.503

[26] Bruneau E, Sutter D, Hume RI, Akaaboune M. Identification of nicotinic acetylcholine receptor recycling and its role in maintaining receptor density at the neuromuscular junction in vivo. J Neurosci 2005; 25:9949-59; PMID:16251443; http://dx.doi.org/10.1523/JNEUROSCI.3169-05.2005

[27] Röder IV, Petersen Y, Choi KR, Witzemann V, Hammer JA, Rudolf R, Hammer 3rd JA, Rudolf R. Role of Myosin Va in the plasticity of the vertebrate neuromuscular junction in vivo. PLoS One 2008; 3:e3871; PMID:19057648; http://dx.doi.org/10.1371/journal.pone.0003871

[28] Stenmark H, Parton RG, Steele-Mortimer O, Lütcke A, Gruenberg J, Zerial M. Inhibition of rab5 GTPase activity stimulates membrane fusion in endocytosis. EMBO J 1994; 13:1287-96; PMID:8137813

[29] Horiuchi H, Lippé R, McBride HM, Rubino M, Woodman P, Stenmark H, Rybin V, Wilm M, Ashman K, Mann M, et al. A novel Rab5 GDP/GTP exchange factor complexed to Rabaptin-5 links nucleotide exchange to effector recruitment and function. Cell 1997; 90:1149-59; PMID:9323142; http://dx.doi.org/10.1016/S0092-8674(00)80380-3

[30] Lanzetti L, Rybin V, Malabarba MG, Christoforidis S, Scita G, Zerial M, Di Fiore PP. The Eps8 protein coordinates EGF receptor signalling through Rac and trafficking through Rab5. Nature 2000; 408:374-7; PMID:11099046; http://dx.doi.org/10.1038/35042605

[31] Wood SJ, Slater CR. Safety factor at the neuromuscular junction. Prog Neurobiol 2001; 64:393-429; PMID:11275359; http://dx.doi.org/10.1016/S0301-0082(00)00055-1

[32] Röder IV, Choi K-RR, Reischl M, Petersen Y, Diefenbacher ME, Zaccolo M, Pozzan T, Rudolf R. Myosin Va cooperates with PKA

RIalpha to mediate maintenance of the endplate in vivo. Proc Natl Acad Sci U S A 2010; 107:2031-6; PMID:20133847; http://dx.doi.org/10.1073/pnas.0914087107

[33] Drachman DB, Adams RN, Stanley EF, Pestronk A. Mechanisms of acetylcholine receptor loss in myasthenia gravis. J Neurol Neurosurg Psychiatry 1980; 43:601-10; PMID:6249894; http://dx.doi.org/10.1136/jnnp.43.7.601

[34] Strack S, Petersen Y, Wagner A, Röder IV, Albrizio M, Reischl M, Wacker IU, Wilhelm C, Rudolf R. A novel labeling approach identifies three stability levels of acetylcholine receptors in the mouse neuromuscular junction in vivo. PLoS One 2011; 6:e20524; PMID:21655100; http://dx.doi.org/10.1371/journal.pone.0020524

[35] Valdez G, Tapia JC, Kang H, Clemenson Jr. GD, Gage FH, Lichtman JW, Sanes JR. Attenuation of age-related changes in mouse neuromuscular synapses by caloric restriction and exercise. Proc Natl Acad Sci U S A 2010; 107:14863-8; PMID:20679195; http://dx.doi.org/10.1073/pnas.1002220107

[36] Carnio S, LoVerso F, Baraibar MA, Longa E, Khan MM, Maffei M, Reischl M, Canepari M, Loefler S, Kern H, et al. Autophagy Impairment in Muscle Induces Neuromuscular Junction Degeneration and Precocious Aging. Cell Rep 2014; 8:1509-21; PMID:25176656; http://dx.doi.org/10.1016/j.celrep.2014.07.061

[37] Wan J, Cheung AY, Fu W-Y, Wu C, Zhang M, Mobley WC, Cheung ZH, Ip NY. Endophilin B1 as a novel regulator of nerve growth factor/ TrkA trafficking and neurite outgrowth. J Neurosci 2008; 28:9002-12; PMID:18768694; http://dx.doi.org/10.1523/JNEUROSCI.0767-08.2008

[38] Libby P, Bursztajn S, Goldberg AL. Degradation of the acetylcholine receptor in cultured muscle cells: selective inhibitors and the fate of undegraded receptors. Cell 1980; 19:481-91; PMID:7357615; http://dx.doi.org/10.1016/0092-8674(80)90523-1

[39] Ikezoe K, Furuya H, Arahata H, Nakagawa M, Tateishi T, Fujii N, Kira JI. Amyloid-beta accumulation caused by chloroquine injections precedes ER stress and autophagosome formation in rat skeletal muscle. Acta Neuropathol 2009; 117:575-82; PMID:19198858; http://dx.doi.org/10.1007/s00401-009-0488-1

[40] Ju JS, Varadhachary AS, Miller SE, Weihl CC. Quantitation of "autophagic flux" in mature skeletal muscle. Autophagy 2010; 6:929-35; PMID:20657169; http://dx.doi.org/10.4161/auto.6.7.12785

[41] Jiang D, Chen K, Lu X, Gao H, Qin Z, Lin F. Exercise ameliorates the detrimental effect of chloroquine on skeletal muscles in mice via restoring autophagy flux. Acta Pharmacol Sin 2014; 35:135-42; PMID:24335841; http://dx.doi.org/10.1038/aps.2013.144

[42] Ju J-S, Fuentealba RA, Miller SE, Jackson E, Piwnica-Worms D, Baloh RH, Weihl CC. Valosin-containing protein (VCP) is required for autophagy and is disrupted in VCP disease. J Cell Biol 2009; 187:875-88; PMID:20008565; http://dx.doi.org/10.1083/jcb.200908115

[43] Kwon I, Lee Y, Cosio-lima LM, Cho J, Yeom D. Effects of long-term resistance exercise training on autophagy in rat skeletal muscle of chloroquine-induced sporadic inclusion body myositis. 2015; 19:225-34; PMID:26525066

[44] Klionsky DJ, Abdelmohsen K, Abe A, Abedin MJ, Abeliovich H, Acevedo Arozena A, Adachi H, Adams CM, Adams PD, Adeli K, et al. Guidelines for the use and interpretation of assays for monitoring autophagy (3rd edition). Autophagy 2016; 12:1-222; PMID:26799652; http://dx.doi.org/10.1080/15548627.2015.1100356

[45] Zhang C, Li A, Zhang X, Xiao H. A novel TIP30 protein complex regulates EGF receptor signaling and endocytic degradation. J Biol Chem 2011; 286:9373-81; PMID:21252234; http://dx.doi.org/10.1074/jbc.M110.207720

[46] Alvarez-Dominguez C, Stahl PD. Increased expression of Rab5a correlates directly with accelerated maturation of Listeria monocytogenes phagosomes. J Biol Chem 1999; 274:11459-62; PMID:10206948; http://dx.doi.org/10.1074/jbc.274.17.11459

[47] Bodine SC, Latres E, Baumhueter S, Lai VK, Nunez L, Clarke BA, Poueymirou WT, Panaro FJ, Na E, Dharmarajan K, et al. Identification of ubiquitin ligases required for skeletal muscle atrophy. Science 2001; 294:1704-8; PMID:11679633; http://dx.doi.org/10.1126/science.1065874

[48] Donà M, Sandri M, Rossini K, Dell'Aica I, Podhorska-Okolow M, Carraro U. Functional in vivo gene transfer into the myofibers of adult skeletal muscle. Biochem Biophys Res Commun 2003; 312:1132-8; http://dx.doi.org/10.1016/j.bbrc.2003.11.032

[49] Choi K-RR, Berrera M, Reischl M, Strack S, Albrizio M, Roder IV, Wagner A, Petersen Y, Hafner M, Zaccolo M, et al. Rapsyn mediates subsynaptic anchoring of PKA type I and stabilisation of acetylcholine receptor in vivo. J Cell Sci 2012; 125:714-23; PMID:22331361; http://dx.doi.org/10.1242/jcs.092361